

Article

What Are the Sectors Contributing to the Exceedance of European Air Quality Standards over the Iberian Peninsula? A Source Contribution Analysis

Pedro Jiménez-Guerrero ^{1,2} 

¹ Department of Physics, Regional Campus of International Excellence Campus Mare Nostrum, University of Murcia, 30100 Murcia, Spain; pedro.jimenezguerrero@um.es; Tel.: +34-868-88-8175

² Biomedical Research Institute of Murcia (IMIB-Arrixaca), 30120 Murcia, Spain

Abstract: The Iberian Peninsula, located in southwestern Europe, is exposed to frequent exceedances of different threshold and limit values of air pollution, mainly related to particulate matter, ozone, and nitrous oxide. Source apportionment modeling represents a useful modeling tool for evaluating the contribution of different emission sources or sectors and for designing useful mitigation strategies. In this sense, this work assesses the impact of various emission sectors on air pollution levels over the Iberian Peninsula using a source contribution analysis (zero-out method). The methodology includes the use of the regional WRF + CHIMERE modeling system (coupled to EMEP emissions). In order to represent the sensitivity of the chemistry and transport of gas-phase pollutants and aerosols, several emission sectors have been zeroed-out to quantify the influence of different sources in the area, such as on-road traffic or other mobile sources, combustion in energy generation, industrial emissions or agriculture, among others. The sensitivity analysis indicates that large reductions of precursor emissions (coming mainly from energy generation, road traffic, and maritime-harbor emissions) are needed for improving air quality and attaining the thresholds set in the European Directive 2008/50/EC over the Iberian Peninsula.

Keywords: air pollution; sensitivity; aerosols; zero-out; Iberian Peninsula



check for updates

Citation: Jiménez-Guerrero, P. What Are the Sectors Contributing to the Exceedance of European Air Quality Standards over the Iberian Peninsula? A Source Contribution Analysis. *Sustainability* **2022**, *14*, 2759. <https://doi.org/10.3390/su14052759>

Academic Editors: Weixin Yang, Guanghui Yuan and Yunpeng Yang

Received: 24 January 2022

Accepted: 24 February 2022

Published: 26 February 2022

Publisher's Note: MDPI stays neutral with regard to jurisdictional claims in published maps and institutional affiliations.



Copyright: © 2022 by the author. Licensee MDPI, Basel, Switzerland. This article is an open access article distributed under the terms and conditions of the Creative Commons Attribution (CC BY) license (<https://creativecommons.org/licenses/by/4.0/>).

1. Introduction

Atmospheric pollution has become one of the most important health and environmental problems worldwide, affecting industrialized and developing countries around the world. Its importance and implications for sustainability have been recognized by the United Nations in their Sustainable Development Goals (SDGs) [1]. Health-relevant indicators of household and ambient pollution exposure and disease burden are included in the formal system of SDG indicators. Targets of particular relevance to ambient and household air pollution include SDG target 3.9.1, which calls for a substantial reduction in the number of deaths and illnesses from air pollution [2,3], or SDG target 11.6.2, which aims to reduce the environmental impact of cities by improving air quality [4,5].

The exposure of humans to air pollution (both photochemical and particulate matter) may be the source of many health problems ([6–12], among many others). The use of chemistry transport models (CTMs) can be a useful tool for assessing these air quality-related health problems. Recently, the premature deaths and the costs of the health impacts of air pollution in Europe were calculated by using ground-level concentrations from different CTMs, indicating that the total number of premature deaths (acute and chronic) ranges from 500,000 to 800,000; their associated costs are around EUR 300 billion [11,13,14].

The Iberian Peninsula (IP), especially, presents serious problems that are related mainly to tropospheric ozone (O₃) [15], sulphur dioxide (SO₂), nitrogen dioxide (NO₂), and particles of different diameters: particulate matter with a diameter of less than 10 (PM₁₀) and more than 2.5 μm (PM_{2.5}) [16]. In this sense, a number of studies have covered the

entire IP using modeling techniques [17–22]. The results of these previous works indicate that achieving the objectives proposed by the EU directives are more difficult in the IP when compared northern countries, partly due to their particular emission distribution [23,24], and partly due to different meteorological situations, namely: (1) a lower precipitation rate (and, hence, a higher resuspension rate due to soil dryness); (2) the increased formation of secondary aerosols associated with the higher temperatures; (3) an enhanced frequency of African dust outbreaks; and (4) the higher occurrence of the recirculation of air masses that prevent air renovation [20,25].

Moreover, air pollution problems will become even more severe under future climates [26–31]. Therefore, reliable estimations of air pollution for present-day conditions and an enhanced understanding of the chemico-physical processes occurring in the atmosphere become essential, not only for informing and alerting the population, but also to understand the causes of those episodes and to implement effective abatement policies.

For that purpose, CTMs are essential for defining, evaluating, and implementing emission abatement plans through the use of sensitivity analysis strategies [32,33]. These strategies have, as a first step, the accurate identification of pollution sources and their individual contributions to the concentrations of atmospheric pollutants. To this end, a wide range of modeling methodologies has been proposed and applied for the apportionment of atmospheric pollutants [34–37]. Particularly, source apportionment relies on the determination of the contribution of different sources to pollutant concentrations by establishing the mass continuity relationships between emissions and concentrations at receptor locations. Sensitivity analyses measure how pollutant concentrations at receptors respond to perturbations at sources. Most of the sensitivity questions are left to modelers since the experimental approach is difficult and expensive.

The traditional approach to sensitivity consists in performing “twin simulations”, with one parameter perturbed [34]. In the case of the most straightforward method to assess sensitivity (brute-force method, BFM), the perturbed parameter is emissions. In the BFM, a model simulation is conducted and repeated with modified emissions, comparing the outputs of the simulations [38,39]. This method is limited because the computational cost depends, in a linear way, on the number of perturbations to examine and the strong influence of the numerical errors when the changes in the concentrations are small. Related to the BFM, the zero-out method [40,41] sets a specific emission sector to zero and measures the change produced in the output concentrations. In this sense, it can be considered as an extreme case of the BFM.

Since the management of air pollutant emissions is one of the predominant factors for abating urban air quality, this work assesses the source contribution of different emitting sectors to the air pollution levels in the IP, taking a particular look at the number of exceedances of air quality limits and thresholds related to health issues. For that, the WRF (meteorology) + CHIMERE (chemistry transport) modeling system has been used for a summer and a winter period over the IP in order to assess air quality-related problems in the area.

2. Materials and Methods

2.1. Modeling System

The modeling system applied consists in the Weather Research and Forecasting (WRF, meteorology) + CHIMERE (chemistry transport model) + EMEP (emissions) methods. The simulations cover the entire IP (excluding a blending area of five grid points), have a resolution of 9 km, and have been run and evaluated on an hourly basis during a period covering a summer and a winter scenario (months of June–July–August 2011, JJA, and December 2011–January–February 2012, DJF). Precisely, the simulation period ranges from 24 May 2011 to 1 September 2011, and from 23 November 2011 to 1 March 2012, with the first week being the spin-up period. The election of the 9-km resolution was conditioned by a compromise between the use of high resolutions and the computational time needed for the ensemble of simulations to be conducted in this analysis.

The regional modeling system consists of the Advanced Research Weather Research and Forecasting (WRF-ARW) Model v3.9.1 [42,43], which provides the meteorology to the CTM. WRF is a fully compressible, Eulerian, non-hydrostatic model that solves the equations that govern the atmospheric motions. A total of 33 vertical layers on sigma coordinates cover the region from the ground level up to 10 hPa. The boundary conditions used for driving the WRF simulations are obtained from the ERA-Interim reanalysis [44] every six hours. WRF fields have been coupled off-line on an hourly basis to CHIMERE CTM [45]. With respect to the CHIMERE configuration, the MELCHIOR2 gas-phase mechanism has been used [46].

Regarding the inclusion of particles within the CTM, CHIMERE includes aerosol and heterogeneous chemistry. Different chemical aerosol components have been included in the model configuration, namely, ammonium, nitrate, sulphate, and organic and elemental carbon with three subcomponents: (1) primary aerosol, (2) secondary anthropogenic, and (3) secondary biogenic subcomponents. Marine aerosols (sea salt) have also been included in the simulation. The aerosol microphysical description is based on a sectional aerosol approach that includes 6 bins using a geometrical progression and ranging from 10 nm to 40 μm . Table 1 summarizes the physico-chemical options for the regional modeling system.

Table 1. Parameterizations of the meteorological and chemistry transport model used in the simulations for the IP.

WRF (Meteorological Model) [42,43]	CHIMERE (Chemistry Transport Model) [45]
Microphysics: WSM6 [47]	Chemical Mechanism: MELCHIOR2 [46]
PBL: Yonsei University [48]	Aerosol chemistry: Inorganic (thermodynamic equilibrium with ISORROPIA module) [49]
Radiation: CAM [50]	Organic aerosol chemistry: [51]
Soil: Noah LSM [52]	Natural aerosols: dust, re-suspended, and inert sea-salt [45]
Cumulus: Kain-Fritsch [53]	Emissions: anthropogenic emissions EMEP [54] + biogenic emissions MEGAN (Model of Emissions of Gases and Aerosols from Nature) [55]
Boundary conditions: ERA-Interim [44]	Boundary conditions: LMDz-INCA+GOCART [56]

Here, the climatological boundary conditions for the CTM are based on the LMDz-INCA global chemistry/climate model [57]. Other considerations to bear in mind, with respect to the boundary conditions, are that (1) the changes in stratospheric ozone are very limited and, hence, are neglected in the simulations, and (2) it has been assumed that long-range transport over the IP is limited and overwhelmed by local processes [58]. This assumption is hampered by the persistent outbreaks of Saharan dust over the IP, which may exert an important influence on the regional PM_{10} levels over Spain and Portugal [59,60]. However, this contribution focuses on a sensitivity analysis of anthropogenic emissions, and hence, the impact of desert sources and their influence on the air quality of the IP is beyond the scope of this work.

Anthropogenic emissions are obtained from the EMEP database [54] and cover the entire period of simulations. Natural emissions have been estimated with the MEGAN model [55] and include species such as monoterpene, isoprene, and other biogenic volatile organic compounds (BVOCs). The meteorological inputs needed for the estimation of emissions are obtained from the WRF simulations previously described.

2.2. Sensitivity Analysis: The Zero-Out Method

The sensitivity analysis methods perturb inputs to the modeling system (e.g., modify the emissions of sulphur oxides) and quantify the response of the model output (e.g., change in sulphate concentration). As commented on before, there are several approaches for a

sensitivity analysis based on the BFM in order to study the contribution from different sources; a zero-out method has been applied in this study because of its simplicity. Here, the methodology includes a base model, run with all emission sources (BC), and ten emission scenarios in which emissions from anthropogenic sources (classified according to the SNAP) are excluded, analogously to previous works [37,61,62].

The zero-out method has been extensively used for source attribution because it seems intuitive and obvious that the removal of an emission source should quantify the corresponding impact of that emission source [40,41,63]. Despite that this methodology is valid and widely used for sensitivity analysis (as in our case), it should be carefully considered for areas with a strong secondary production, because the sum of zero-out impacts over all sources may not be exactly equal to the total concentration when considering non-linear systems as those represented by atmospheric processes [34]. In this sense, Clappier et al. [36] warn that, when the non-linearity of the relationship between concentrations and emissions is noticeable, source apportionment methods may not be appropriate to assess the impact of mitigation or abatement strategies. When non-linearity is limited or negligible, source apportionment methods may be acceptable, bearing in mind the complexity of the models involved in the representation of air pollution.

Since our objective is to conduct a source apportionment analysis for the IP, the zero-out method has been applied to all the SNAP activities, including anthropogenic sources (Table 2). The sensitivity to air pollution levels of these sources is covered and identified in the simulations (harbors and ships, industries, road transport, central heating, agriculture, etc.).

Table 2. Tags for the different simulations included in this contribution. The scenarios are run while zeroing-out the emissions specified by the SNAP sector.

SNAP	Emissions Zeroed-Out
SNAP1	Combustion in energy and transformation industries
SNAP2	Non-industrial combustion plants, including private wood combustion
SNAP3	Combustion in manufacturing industry
SNAP4	Production processes
SNAP5	Extraction and distribution of fossil fuels and geothermal energy
SNAP6	Solvents and other product use
SNAP7	Road transport
SNAP8	Other mobile sources and machinery (excl. international ship traffic)
SNAP9	Waste treatment and disposal
SNAP10	Agriculture
Base Case (BC)	No emissions zeroed-out

3. Results

3.1. Evaluation of the Modeling Results

Despite that the goal of this contribution is not to provide a comprehensive evaluation of the air quality concentrations simulated by WRF + CHIMERE, the results from the monitoring network EMEP have been used to characterize the skill of the model for reproducing the concentrations of air pollutants (EMEP data available online at: <http://www.emep.int> (accessed on 8 May 2012); see [64] for further details). The ten stations with simultaneous data of tropospheric O₃, NO₂, and PM₁₀ in the IP (SO₂ and PM_{2.5} have been excluded because of the scarcity of data for the target period) have been used for the model evaluation. Their location is shown in Figure 1.



Figure 1. EMEP stations included for the model validation.

The available EMEP measurements were filtered before comparing the model results with EMEP data in order to remove uncertain data (for instance, those data before a calibration of equipment or after an interruption was eliminated). In addition, after the EMEP data is filtered, the criteria of temporal coverage >85% were selected for measurement sites. Since EMEP stations are located far from large emission sources (more than 10 km), the data are assumed to fit the resolution of the model used for regional background concentrations ([64] and references therein).

A number of common metrics were used to examine the model skills, differencing between gas-phase and particulate matter. For gases, two scores have been selected: mean normalized gross error (MNGE)—which indicates the performance of the simulations to represent the magnitude of the observation—and the mean normalized bias error (MNBE)—another common parameter that reveals the departure between observations and modeling data. These provide a useful quantification of the overall under- or overestimations of the model.

As for the particulate matter evaluation, a number of authors (e.g., [16,65–67], among many others) suggested using the mean fractional bias (MFB) and the mean fractional error (MFE) instead of MNBE or MNGE (Table 3). Boylan and Russell [65] propose that a model performance goal is met when both the MFE and MBE are less than or equal to 50% and $\pm 30\%$, respectively, and a model performance criterion is met when the MFE $\leq 75\%$ and MFB is less than or equal to $\pm 60\%$.

Table 3. Statistical figures used in the evaluation of the WRF + CHIMERE modeling system. N: number of observations available. C_{mod} : model concentration. C_{obs} : observation concentration.

Value	Formula	Range
Model Mean (MM)	$\frac{1}{N} \sum C_{mod}$	$0, +\infty$
Observations Mean (OM)	$\frac{1}{N} \sum C_{obs}$	$0, +\infty$
Mean Normalized Bias Error (MNBE)	$\frac{1}{N} \sum \frac{(C_{mod} - C_{obs})}{C_{obs}}$	$-\infty, +\infty$
Mean Normalized Gross Error (MNGE)	$\frac{1}{N} \sum \frac{ C_{mod} - C_{obs} }{C_{obs}}$	$0, +\infty$
Mean Fractional Bias (MFB)	$\frac{1}{N} \sum \left(\frac{(C_{mod} - C_{obs})}{\left(\frac{C_{mod} + C_{obs}}{2}\right)} \right)$	$-200, +200$
Mean Fractional Error (MFE)	$\frac{1}{N} \sum \left(\frac{ C_{mod} - C_{obs} }{\left(\frac{C_{mod} + C_{obs}}{2}\right)} \right)$	$0, +200$

Therefore, MNBE and MNGE have been used for gaseous pollutants, while for particulate matter, the MFB and MFE have been utilized. A general pattern of the air pollution levels provided by WRF + CHIMERE simulations can be found in Figure 2. Maximum O₃ concentrations are modeled for summertime in the easternmost part of the IP, with ground levels that exceed 120 µg m⁻³ as the daily mean in Catalonia (northeastern IP). For NO₂, monthly means can be as high as 50 µg m⁻³ in the largest cities of the peninsula (e.g., Madrid, Lisbon, Porto) and in an industrial area such as Algeciras Bay (southernmost part of the IP), where industrial emissions are increased by port and maritime activity. The Algeciras port (the second most important port of Spain), located at the head of the bay, has a strategic importance in terms of the maritime traffic of fuel and general supplies [68]. Hence, the presence of this port makes the area of the Algeciras Bay a high risk environment for pollution derived from its commercial activities. For SO₂, besides Algeciras, levels are over 20 µg m⁻³ downwind of several power plants (As Pontes, in northern Spain; and Andorra (Teruel), in the eastern IP) that burn coal for the generation of electricity [69,70]. Last, particulate matter does not exhibit a clear spatial pattern in the IP. The spatial patterns depend both on the industrialization of the regions, especially regarding inorganic particulate matter, and the Saharan dust outbreaks [20]. In this sense, PM_{2.5} and PM₁₀ seasonal patterns showed maximum concentrations during summertime, as is also indicated by the scientific literature.

Regarding model validation, overall, negative fractional biases are calculated for PM₁₀ and NO₂, while positive deviations for O₃ are obtained when comparing the base-case simulation to EMEP stations (Table 4).

Table 4. Model evaluation against EMEP stations. (Top) Summer (JJA) and (bottom) winter (DJF).

Summer	JJA 2011	PM ₁₀		NO ₂		O ₃	
Code	Station Name Performance Criteria	MFB (%) ≤±60% ¹	MFE (%) ≤+75% ¹	MNBE (%)	MNGE (%) ≤+50% ²	MNBE (%)	MNGE (%) ≤+50% ²
ES07	Víznar	−38.8	68.8	−28.9	41.9	23.1	24.9
ES08	Niembro	−9.0	42.6	−19.0	41.6	22.1	22.1
ES09	Campisábalos	−54.0	54.1	−35.8	49.0	5.0	25.7
ES10	Cabo de Creus	−41.9	43.7	−15.2	33.6	1.5	26.7
ES11	Barcarrota	−58.9	68.9	−45.5	46.1	22.3	26.4
ES12	Zarra	−52.5	53.0	−46.8	49.3	20.3	24.2
ES13	Peñausende	−55.1	57.0	−28.5	59.4	11.2	12.5
ES14	Els Torms	−48.6	49.2	−34.7	44.9	20.3	21.0
ES15	Risco Llano	−52.5	62.5	−47.3	47.3	24.9	25.6
ES16	O Saviñao	6.8	41.8	18.3	40.9	32.3	33.9
Winter	DJF 2011	PM ₁₀		NO ₂		O ₃	
Code	Station Name Performance Criteria	MFB (%) ≤±60% ¹	MFE (%) ≤+75% ¹	MNBE (%)	MNGE (%) ≤+50% ²	MNBE (%)	MNGE (%) ≤+50% ²
ES07	Víznar	−55.7	55.8	−41.8	48.3	23.0	25.9
ES08	Niembro	−17.1	21.7	−17.1	21.7	8.3	8.3
ES09	Campisábalos	−28.7	57.2	−36.1	48.0	2.0	15.0
ES10	Cabo de Creus	−34.8	35.2	−17.8	27.7	2.2	25.5
ES11	Barcarrota	−21.6	34.9	−13.0	31.9	23.6	24.9
ES12	Zarra	−20.7	34.2	−20.7	34.2	29.8	29.8
ES13	Peñausende	−8.3	35.4	0.3	38.5	19.8	20.2
ES14	Els Torms	−34.3	45.8	−31.3	44.2	30.2	32.4
ES15	Risco Llano	−37.7	58.0	−39.6	48.9	26.0	26.6
ES16	O Saviñao	−11.3	28.2	−7.8	26.3	17.1	17.3

MFB: Mean Fractional Bias; MFE: Mean Fractional Error; MNGE: Mean Normalized Gross Error; MNBE: Mean Normalized Bias Error. ¹ Boylan and Russell [65]; ² EU Directive 2008/50/EC Uncertainty.

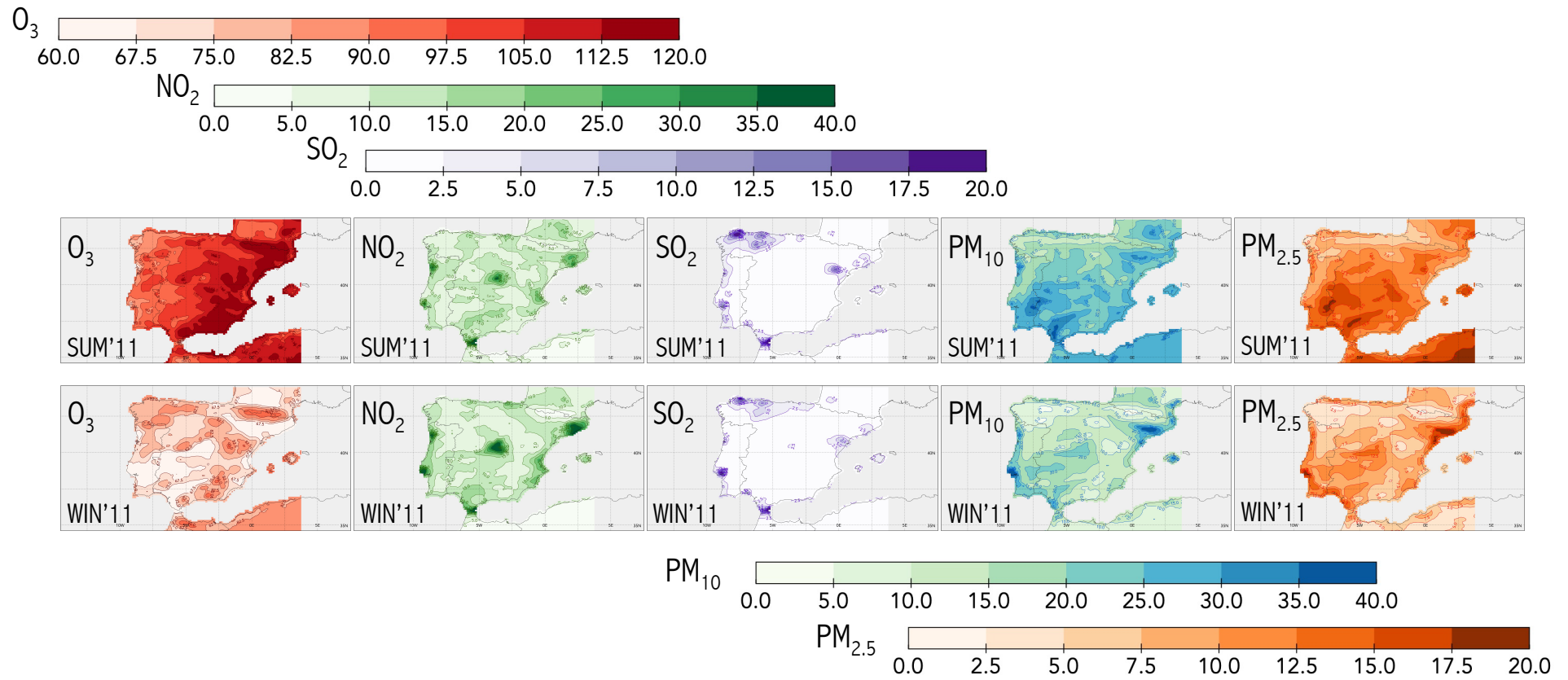


Figure 2. Summer (top) and winter (bottom) 2011 average concentration of tropospheric ozone (red), nitrogen dioxide (green), sulphur dioxide (purple), PM_{10} (blue), and $PM_{2.5}$ (orange). All units in $\mu\text{g m}^{-3}$.

With respect to gaseous pollutants, the WRF + CHIMERE model presents a MNGE under 50% for NO₂, which is the value set by the EU Directive 2008/50/EC uncertainty criteria. However, this pollutant is underestimated in both seasons and in all stations (except for in summer in ES16-O Saviñao and winter in ES13-Peñausende), possibly due to uncertainties in emission inventories [71] and the relatively coarse horizontal resolution used, which represents only partially the spatial gradient of the emissions [72]. Negative biases vary between −8% in wintertime in ES16-O Saviñao (northwestern Spain) and −47% in ES12-Zarra (at the Levantine Spanish coast). Tropospheric O₃ is generally overestimated (bias under +20% in summer and under +30% during wintertime). This is related to the NO₂ underestimation, limiting the titration of tropospheric O₃ by NO₂. Moreover, the CHIMERE lateral boundary conditions for O₃ are overestimated [57,72], especially during wintertime, and therefore, the positive biases during the cold season (ranging from 2% at ES09-Campisábalos to 30% at ES14-Els Torms, northeastern Spain) are attributable to the overestimation of the background concentrations at the boundaries of the domain.

For particulate matter (PM₁₀), the magnitude of the MFB and MFE are similar in both seasons, meeting the performance criteria established by Boylan and Russell [65] for all stations and during all seasons. There is a pervasive tendency to underestimate PM₁₀ levels (negative MFB in all stations and both seasons, except for station ES16-O Saviñao, northwestern Spain, in summer). This summer MFB ranges from −9% in ES08-Niembro station (northern Spain) to −59% in ES11-Barcarrota (southwestern Spain). In wintertime, the maximum MFB is −56% in ES07-Víznar (southern Spain), while the minimum MFB is estimated in ES13-Peñausende (western Spain, near the Portuguese border) as −8%. More interesting is the fact that high MFEs are found in ES07-Víznar station for both seasons (68% in summer and 56% in winter). The MFB is strongly negative and almost coincident with the MFE (e.g., −56% for the MFB error in wintertime and 56% for the MFE during this season). This could be caused by the high contribution of Saharan dust at this location [25,73], which is pervasively underestimated by CTMs in southern Mediterranean stations, especially regarding the peak levels [74–76].

3.2. Source Contribution

Figures 3 and 4 represent the results of the source contribution experiment for summertime and wintertime, respectively. The information shown in those Figures is quantified in Table 5, which indicates the relative reductions in the areas with the worst air quality in the entire IP (that is, reductions in those locations of the target domain where the daily mean and the daily mean of max. 1-hr ground-level air quality concentrations are the highest). The results are shown with respect to the base-case scenario (BC), and focus only on anthropogenic sectors (that is, excluding, for instance, the contribution of background concentrations or external transport, which cannot be controlled in abatement strategies). Overall, Table 5 indicates that the maximum reductions in air pollution levels are achieved when zeroing-out three SNAP sectors, as expected from the scientific literature: combustion in energy and transformation industries (SNAP1), road transport (SNAP7), and other mobile sources (SNAP8). The most important added value of this contribution, nonetheless, is the quantification of the respective contributions of these aforementioned sectors. For the sake of brevity, our analysis below focuses only on the assessment of the contribution from these sectors (despite that agriculture, SNAP10, may play also an important role for SO₂ and particulate matter).

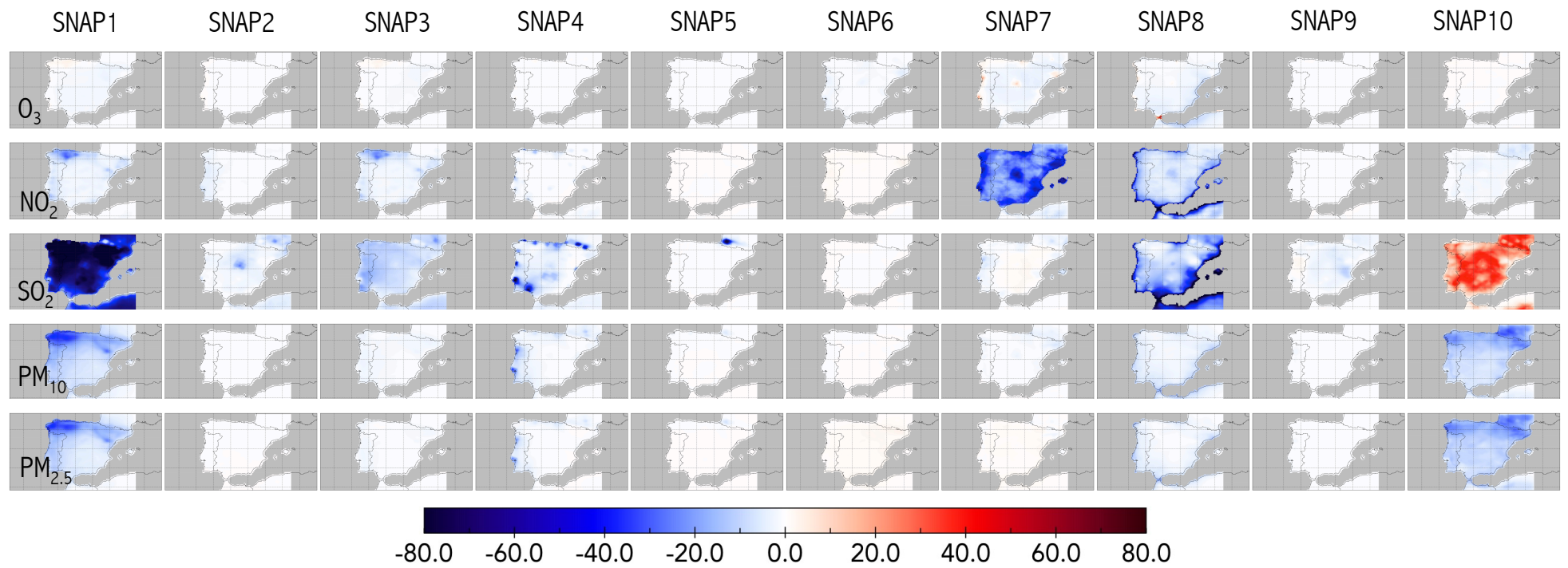


Figure 3. Relative contribution (%) of each anthropogenic SNAP sector to the daily mean levels of pollutants over the IP during summertime (JJA) 2011.

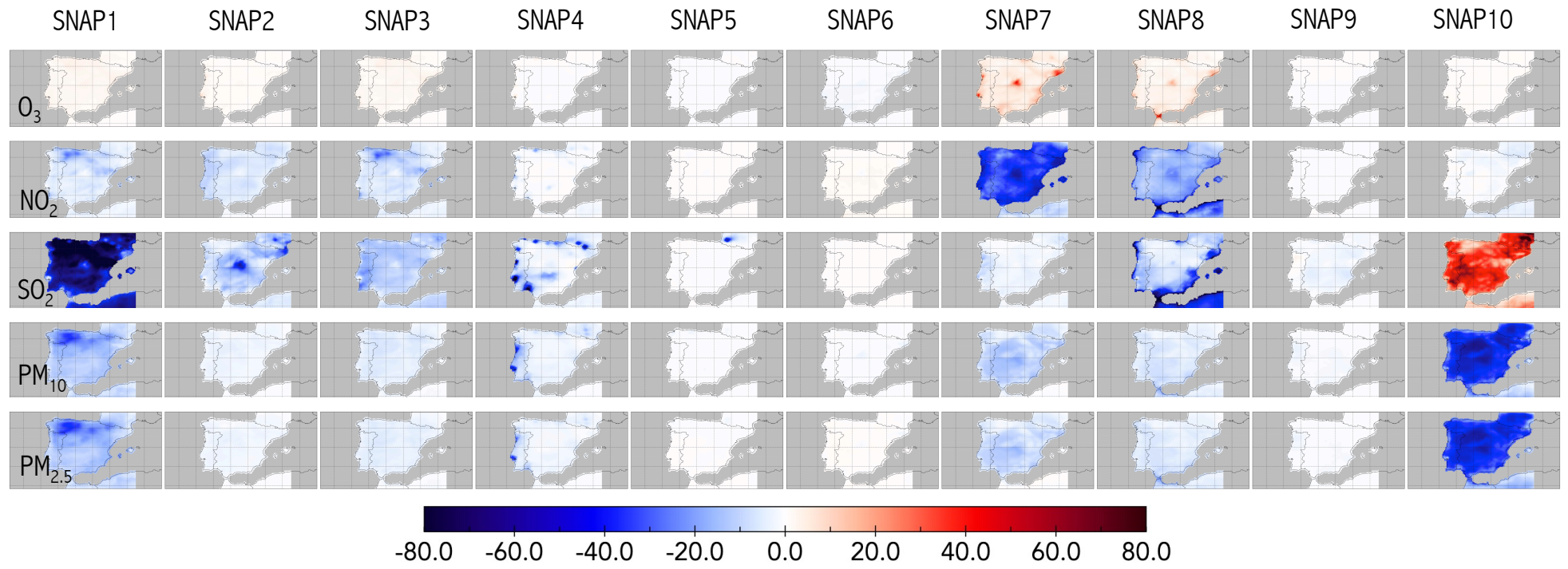


Figure 4. Id. Figure 3 but for wintertime (DJF).

Table 5. Variation in the mean and maximum levels of atmospheric pollutants over the entire IP when zeroing-out the different SNAP sectors (base case minus zeroed-out SNAP sector simulation; hence, a positive value indicates an improvement in air quality).

Summer	Summer (JJA)				
	Concentration	Base Case	w/o SNAP	Reduction	
Pollutant	Mean ($\mu\text{g m}^{-3}$)	Max ($\mu\text{g m}^{-3}$)	Zero-out sector	Mean	Max
Tropospheric ozone, O_3	132.5	164.6	SNAP7	2.3%	5.7%
			SNAP8	5.0%	1.9%
Nitrogen dioxide, NO_2	66.6	124.2	SNAP8	47.4%	37.1%
Sulphur dioxide, SO_2	33.0	70.7	SNAP1	2.0%	2.4%
			SNAP8	40.9%	40.3%
Particulate matter $\phi < 10 \mu\text{m}$, PM_{10}	38.7	62.2	SNAP1	6.2%	4.3%
			SNAP8	7.0%	2.6%
			SNAP10	5.7%	2.6%
Particulate matter $\phi < 2.5 \mu\text{m}$, $\text{PM}_{2.5}$	19.7	29.3	SNAP1	0.0%	4.8%
			SNAP8	0.0%	2.4%
			SNAP10	5.1%	4.8%
Winter	Winter (DJF)				
	Concentration	Base Case	w/o SNAP	Reduction	
Pollutant	Mean ($\mu\text{g m}^{-3}$)	Max ($\mu\text{g m}^{-3}$)	Zero-out sector	Mean	Max
Tropospheric ozone, O_3	95.8	103.7	SNAP7	−1.2%	−2.3%
			SNAP8	12.3%	9.7%
Nitrogen dioxide, NO_2	60.0	95.4	SNAP7	32.9%	17.7%
Sulphur dioxide, SO_2	33.0	70.7	SNAP1	4.5%	3.6%
			SNAP8	2.5%	22.2%
Particulate matter $\phi < 10 \mu\text{m}$, PM_{10}	54.3	93.5	SNAP4	6.6%	17.5%
			SNAP7	3.9%	3.3%
			SNAP10	14.0%	13.8%
Particulate matter $\phi < 2.5 \mu\text{m}$, $\text{PM}_{2.5}$	21.0	34.4	SNAP1	4.7%	3.7%
			SNAP7	5.3%	4.0%
			SNAP10	16.1%	14.3%

For tropospheric O_3 , on-road traffic (SNAP7) is the most important contributor in summertime. The highest daily mean levels of tropospheric O_3 during summer ($133 \mu\text{g m}^{-3}$) reduce by 2%, while 1-h maximum concentrations ($165 \mu\text{g m}^{-3}$) decrease by 6%. In addition, zeroing-out other mobile sources (SNAP8) reduces the highest daily mean and 1-h maximum O_3 summertime levels by 5% and 2%, respectively. On the contrary, zeroing-out on-road traffic (SNAP7) during winter slightly contributes to an increase in tropospheric O_3 concentrations (1% and 2% in wintertime, mean and maximum concentration, 96 and $104 \mu\text{g m}^{-3}$, respectively), but this increase does not involve the exceedance of the objective value, as will be shown later in Section 3.4.

The response of tropospheric O_3 to changes in their precursors (nitrogen oxides, NO_x , and volatile organic compounds (VOCs)) has been widely covered in the scientific literature, and particularly over the IP [77,78]. Overall, under certain conditions, O_3 concentrations are reduced when NO_x emissions decrease. This chemical regime is denoted as NO_x -sensitive conditions. Conversely, under other conditions, tropospheric O_3 reduces its levels when VOC emissions (particularly, non-methane volatile organic compounds, NMVOCs) are reduced, and might even increase its concentration when NO_x emissions are mitigated. This regime is known as VOC-sensitive conditions. These O_3 sensitivity regimes can help with explaining the variations in the levels of this pollutant over the Iberian Peninsula. Namely, the increase in winter O_3 mean levels in the Algeciras Bay when zeroing-out the

SNAP8 emissions and the shipping route of the Strait of Gibraltar is a direct consequence of the high NO₂ concentrations over this target area, associated with the important NO_x emissions of the SNAP8 sector. When removing shipping emissions, mostly NO_x emissions are removed, and hence, the increase of tropospheric O₃ reveals the strong VOC-limited chemical regime for O₃ formation in that area. At low NMVOC/NO_x ratios, the results are sensitive to the concentrations of volatile compounds [77,79,80], and hence, an accurate amount of NMVOC ship emissions is essential for studying and understanding their possible impact on the O₃ levels, especially in such polluted areas as the Mediterranean Sea.

The most important pollutant coming from on-road traffic (SNAP7) is NO₂, and this sector is the dominant source in the largest populated areas of the IP. For NO₂, reductions in the highest daily mean levels in the target domain are around 10 µg m⁻³ in wintertime (up to 30 µg m⁻³ as daily mean levels in summertime), especially in the Barcelona and Madrid Greater Areas, and the axis of highways covering the Levantine and Western areas of the IP (Barcelona–Murcia and Porto–Lisbon, in that order), representing almost 50% of the NO₂ levels for this pollutant in summertime (Figure 3) and over 60% in wintertime at those sites and roads (Figure 4).

Other mobile sources (SNAP8) also largely contribute to NO₂ and SO₂ over the peninsula (playing also a role regarding the PM₁₀ levels). In this sense, SNAP8 is responsible for 47% and 37% of the daily mean (67 µg m⁻³) and maximum (124 µg m⁻³) levels of NO₂ in the target domain in summer (12% and 10% in winter; the concentrations are 60 and 95 µg m⁻³ for mean and maxima, in that order). For wintertime, on-road traffic contributes to highest mean and maximum NO₂ concentrations by 33% and 18%, respectively. Last, as shown in Figure 3, combustion in energy and transformation industries (SNAP1) can add up to 4 µg m⁻³ in the area close to power plants, representing up to 10% of NO₂ levels in those areas. However, Table 5 indicates that the contribution of this SNAP to maximum values is not significant when considering the entire IP.

For SO₂, combustion in energy and transformation industries (SNAP1) represents an important source of the contribution to the levels of this pollutant. The simulations shown in Figure 3 for summertime and Figure 4 for wintertime feature strong reductions in SO₂ ground-level concentrations over land when zeroing-out SNAP1 (mean reduction, 2.5 µg m⁻³, reaching 7 µg m⁻³ in large emitting areas associated with coal combustion). These results are in agreement with Valverde et al. [70], who indicate that the contribution to SO₂ from power plants in the IP ranges from 2 to 25 µg m⁻³.

This energy sector contribution can be as much as 60% over the IP, except in the Mediterranean coastal areas, where the reduction is around 30–40%. In summertime, the contribution of energy facilities can add up to 2% to the mean and maximum levels (39 and 141 µg m⁻³, in that order) of SO₂ simulated by the model. It is, however, SNAP8 (other mobile sources) which contributes most to summer SO₂ highest mean and maximum levels (41% and 40%, respectively). The winter contribution is much lower, with SNAP8 representing only 3% and 22% of the highest winter SO₂ mean and maxima (33 and 71 µg m⁻³, in that order). Analogous contributions of SNAP1 can be found for winter in the target domain (5 and 4%). The contribution of harbor emissions to sulphur dioxide levels may reach 50% in the Iberian Levantine coast, both for summertime and wintertime (Figures 3 and 4), reaching up to 2 µg m⁻³ in the western Mediterranean areas, and around 5 µg m⁻³ in the Algeciras harbor and Gibraltar (southern IP) during summertime, highlighting the importance of this sector.

With respect to PM₁₀, Table 5 indicates that, albeit for summertime the sector with the largest contribution to highest daily mean and maximum levels (39 and 62 µg m⁻³) is combustion in energy and transformation industries (SNAP1) (6.2% and 4.3%), production processes (SNAP4) is the source that contributes most during wintertime to the PM₁₀ highest mean and maxima (54 and 93 µg m⁻³), representing 7% and 18% of those levels. The second largest contributor to PM₁₀ is SNAP8 (other mobile sources) in summer (7% and 3% to highest mean and maxima) and SNAP7 (road traffic) in winter (4% and 3%). It is noticeable that removing agriculture emissions (SNAP10) contributes to a decrease in

PM levels and a simultaneous increase in SO₂ concentrations both for summer (Figure 3) and winter (Figure 4), since zeroing-out the most important contributor to NH₃ emission hampers the formation of ammonium sulphate, and hence, more SO₂ is available in the gas-phase [20,27,81]. Analogous results can be found for PM_{2.5}, but with an enhanced contribution of agriculture (SNAP10) to the PM_{2.5} daily mean and maxima, which can reach 16% and 14%, respectively.

3.3. Source Contribution at Critical Selected Sites

Figure 5 shows the Air Quality Index (AQI) in the IP (estimated from EPA Air Quality Index [82]) in order to assess the most critical areas in the target domain regarding air pollution. In this index, the concentrations that correspond to an AQI value of 100 are those established as the standards of the European Union, compiled in Directive 2008/50/EC. The election of the AQI in this contribution is not critical, since only the areas with the poorest air quality are searched to calculate the source contribution at those particular locations.

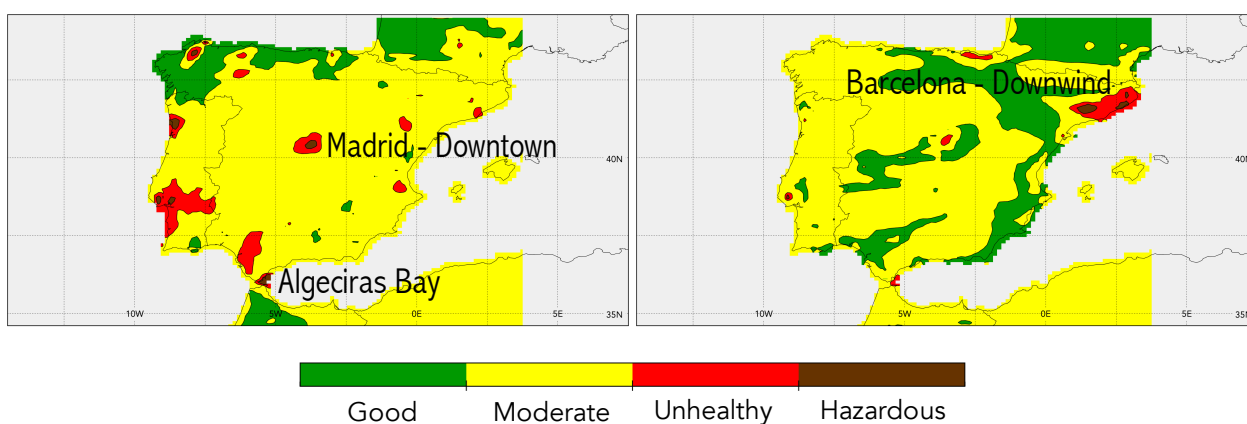


Figure 5. Total air quality indexes (AQI_{total}) for summer (JJA) (left) and winter (DJF) (right), indicating the most polluted areas of the IP (AQI = hazardous).

The AQI has been estimated individually for all pollutants with regulatory values included in this contribution (O₃, NO₂, SO₂, PM₁₀, and PM_{2.5}) and the AQI_{total} (shown in Figure 5) has been estimated as the highest value among all individual indexes. During the summer and winter periods, air quality was hazardous in the two largest Spanish cities (Madrid and Barcelona) and the industrial-harbor area of Algeciras Bay, located in southern Spain (Figure 5). Therefore, this section is devoted to the analysis of the source apportionment at these locations in order to shed some light on the causes of the strategy to abate those pollutants. For that, the point with the worst air quality in a domain of 100 km², centred over Madrid, Barcelona, and Algeciras, respectively, has been selected for further analysis.

For gas-phase pollutants, Figure 6 (left) indicates that most of summertime tropospheric O₃ comes from the “Other” sector at all the three sites. This “Other” contribution is not estimated by zeroing-out any emission sector, but estimated as the difference between the BC and the addition of all anthropogenic sources. Therefore, it includes the contribution of different processes (e.g., long-range transport, background levels, stratosphere–troposphere exchange, etc.).

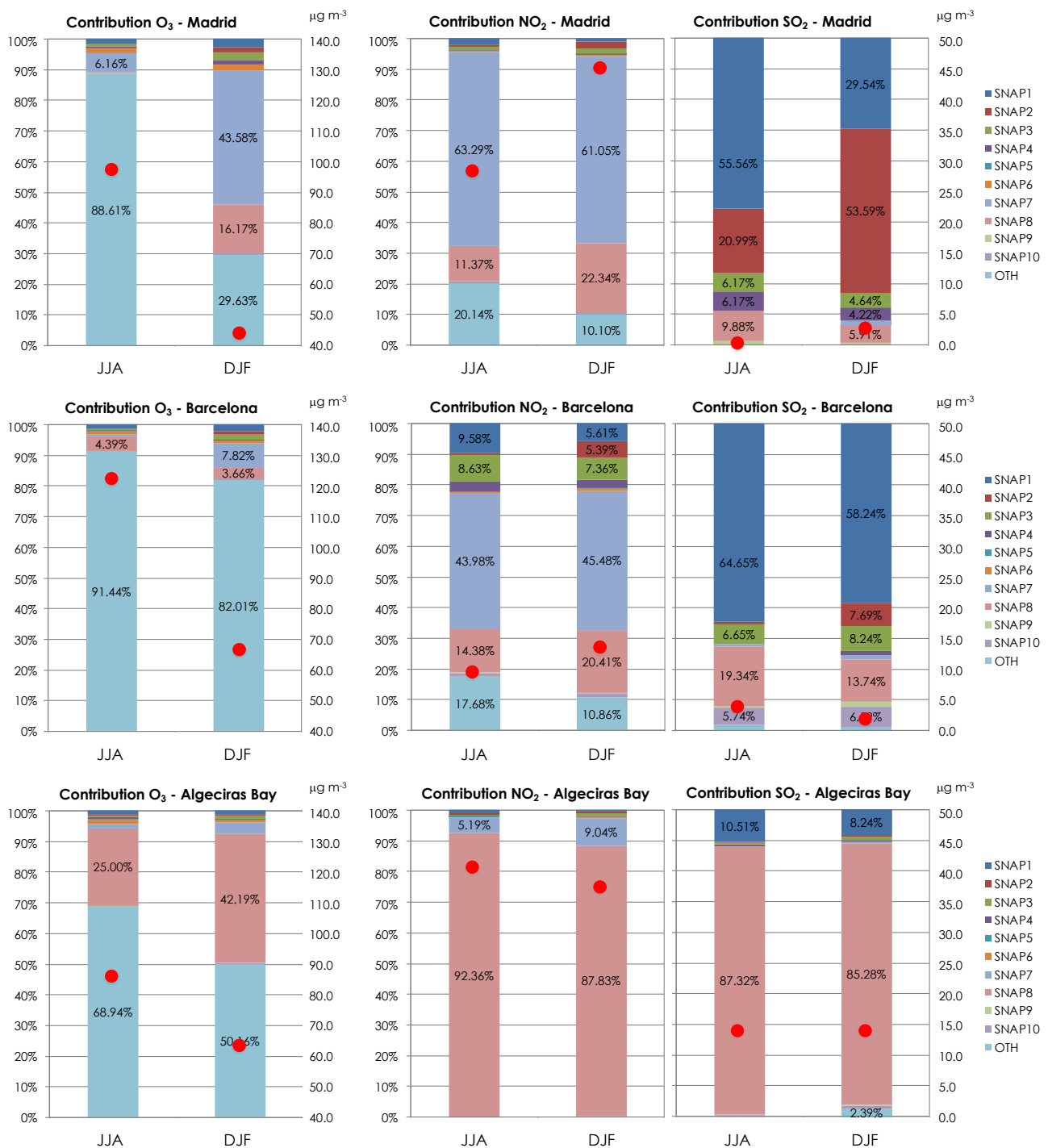


Figure 6. (Left axis) Relative contribution (%) of each anthropogenic SNAP sector to the daily mean levels of O₃ (left), NO₂ (center), and SO₂ (right) over the most polluted areas of the IP (Madrid, top; Barcelona, center; Algeciras Bay, bottom). (Right axis) Red dot stands for the mean concentrations of O₃ (left), NO₂ (center), and SO₂ (right) in µg m⁻³.

During summer (winter), this contribution can be as large as 88% (30%) in Madrid, 91% (82%) in Barcelona, and 69% (50%) in Algeciras Bay. These numbers are in agreement with previous works. For instance, the background values contribute with more than 50% to the O₃ concentration measured in the westernmost region of the IP [83]. Moreover, the importance of intercontinental ozone transport in the ground levels of ozone over Europe has been highlighted [84], and can be as high as 10–16 ppb (20–32 µg m⁻³). In Barcelona and

the Algeciras Bay, the anthropogenic sector contributing most to tropospheric O₃ levels is SNAP8 (other mobile sources), especially related to shipping emissions in the area. SNAP8 adds up 4% (25%) and 4% (42%) of summer and wintertime O₃, respectively, in Barcelona (Algeciras). These results are in agreement with those of the literature [85,86]. These works find out that shipping emissions increase ground levels of summer tropospheric O₃ by 5 to 10% in the Mediterranean sea. This may be caused by the large NO₂ emissions of ships, which can enhance the production of ozone [87]. Last, SNAP7 (road traffic) has a limited contribution to summertime O₃ levels in Madrid and Barcelona, around 8%, which is in a strong agreement with previous works [88].

With respect to NO₂ (Figure 6, center), on-road traffic (SNAP7) is the sector with the highest contribution to the surface levels of NO₂ in Madrid and Barcelona (over 60% in Madrid and over 44% in Barcelona for both seasons), followed by SNAP8 (other mobile sources). While for Barcelona, it is the shipping and maritime activity that contributes most to SNAP8 (being responsible for 14% and 20% of summer and winter NO₂ levels in the city), in Madrid, the contribution of SNAP8 (11% in summer and 22% in winter) comes mainly from the activity of the Madrid airport. In Algeciras, around 90% of NO₂ levels can be attributed to the shipping sector, both in summertime and wintertime. The contribution of SNAP8 is very similar in Algeciras Bay for SO₂ levels (the source apportionment indicates that over 85% of SO₂ mean levels in Algeciras come from SNAP8) (Figure 6, right). However, in the city of Madrid, most of the summer (winter) SO₂ has an origin in combustion during energy-generation activities (SNAP1): 56% (30%) of monthly means for summertime (wintertime), followed by non-industrial combustion plants, including private wood combustion—SNAP2—(21%/54% of summer/winter levels). In Barcelona, SNAP1 is also responsible for around 60% of SO₂ levels, with a limited contribution of shipping emissions (19% for summertime and 14% during winter) and agriculture—SNAP10—(around 6% for both seasons). It should be highlighted that the levels of SO₂ in the urban areas of Madrid and Barcelona are very low, with mean monthly concentrations under 5 µg m⁻³.

Figure 7 indicates the results regarding the contribution of each SNAP sector to the daily mean levels of PM_{2.5} (left) and PM₁₀ (right). The most important contributor to PM_{2.5} and PM₁₀ concentrations in Madrid, Barcelona, and Algeciras is the sector “Other”, highlighting the importance of external sources to the domain during summertime (e.g., Saharan dust transport). In this sense, the outside contribution represents 72% (73%), 59% (63%), and 52% (57%) of summertime PM_{2.5} (PM₁₀) levels in Madrid, Barcelona, and Algeciras, respectively. However, this contribution is much lower for wintertime, when the external contribution accounts for only 16% (7%), 31% (29%), and 35% (29%) of PM_{2.5} (PM₁₀) levels at the aforementioned sites. The fact that the PM₁₀ contribution is larger than PM_{2.5} for summertime, but lower for wintertime, points to an important role of dust outbreaks over the IP during the summer months, as aforementioned [25,73].

Agriculture (SNAP10) effects on particulate matter levels are much larger in wintertime than during summertime. SNAP10 has a larger contribution to summer particles in Barcelona (18% for PM_{2.5} and 16% for PM₁₀) than in the case of Madrid (6% for PM_{2.5} and PM₁₀) or Algeciras (14% and 10% for PM_{2.5} and PM₁₀, respectively). These contributions increase notably for wintertime, with agriculture being the most important contributor to wintertime PM_{2.5} and PM₁₀ levels in Madrid (49% and 52%, respectively) and Barcelona (39% and 40%).

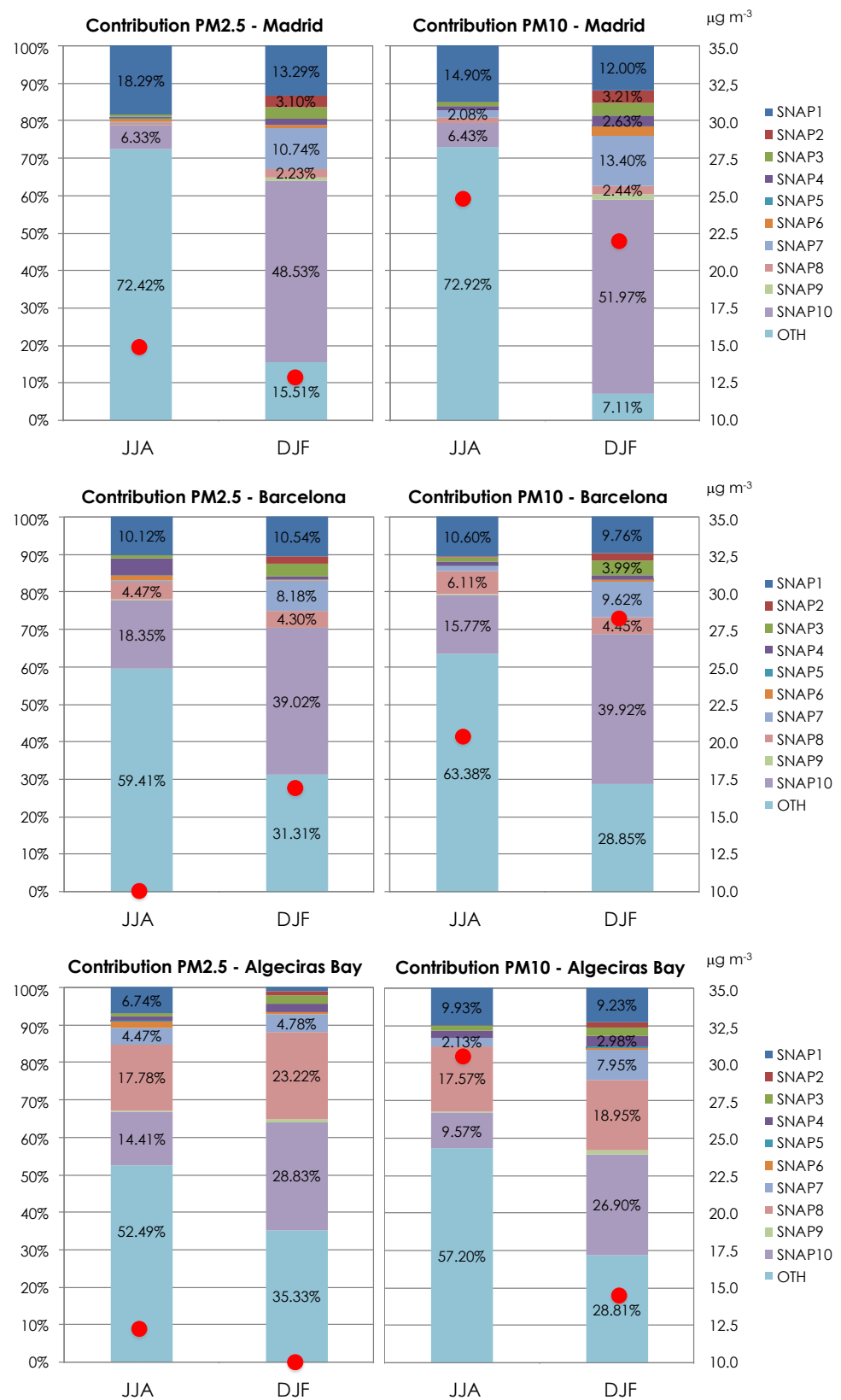


Figure 7. (Left axis) Relative contribution (%) of each anthropogenic SNAP sector to the daily mean levels of PM_{2.5} (left) and PM₁₀ (right) over the most polluted areas of the IP (Madrid, top; Barcelona, center; Algeciras Bay, bottom). (Right axis) Red dot stands for the mean monthly concentrations of PM_{2.5} (left) and PM₁₀ (right) in $\mu\text{g m}^{-3}$.

Combustion in energy and transformation industries (SNAP1) also notably contributes to particle levels in the city of Madrid (PM_{2.5}: 18% for summer and 13% for winter; PM₁₀: 15% and 12% in summer and winter, in that order), Barcelona (PM_{2.5}: 10% for summer and 11% for winter; PM₁₀: 11% and 10% in summer and winter, respectively), and Algeciras (PM_{2.5}: 7% and 1% for summer/winter; PM₁₀: 10% and 9% in summer and winter, in that order). On-road traffic (SNAP7) is only noticeable for wintertime PM_{2.5}(PM₁₀) concentrations, being 11% (13%), 8% (10%), and 5% (8%) in Madrid, Barcelona, and Algeciras, while the contributions of SNAP8 (other mobile sources) are very high in Algeciras, being the second largest contributor for particulate matter both in summer (18% for PM_{2.5} and PM₁₀) and winter (23% and 19% for PM_{2.5} and PM₁₀, respectively), due to the presence of important harbor/industrial activity in the area [89,90]. Over a coastal area such as Barcelona, the estimated contribution of harbor emissions to the urban background reached 9–12% for PM₁₀ and 11–15% for PM_{2.5} [91]. Our results are in agreement with those numbers (despite being slightly lower), since the estimations of the contribution of SNAP8 to PM_{2.5}(PM₁₀) background levels in Barcelona is around 4–6%. This contribution is linked both to primary emissions from fuel oil combustion but also to the formation of secondary aerosols from gas-phase precursors.

3.4. Response of Air Quality Exceedances to Zeroed-Out Emissions

It is important to characterize the contribution of each emitting sector to air pollution not only from the point of view of the percent contribution to mean air quality levels, but also to attribute the role of those sources in the exceedances of limit values for the protection of human health. In this sense, Table 6 summarizes the contribution over the entire IP of each SNAP sector (only for those sectors with significant variations with respect to the BC) to the number of exceedances of different target values selected: objective value for O₃, 120 µg m⁻³, 8 h; limit value for NO₂, 200 µg m⁻³, 1 h, not to be exceeded (n.t.b.e.) more than 3 times a calendar year; limit value for SO₂, 125 µg m⁻³, 1 day, n.t.b.e. more than 3 times a calendar year; limit value for PM₁₀, 50 µg m⁻³, 1 day, n.t.b.e. more than 35 times a calendar year. Additionally, the limit value for PM_{2.5}, 25 µg m⁻³, 1 calendar year, was explored, but as we have only simulated summer and winter periods, this latter limit value cannot be assessed.

With respect to the exceedance of the target, limit, and threshold values set in the Directive 2008/50/EC, Table 6 indicates a clear improvement in the O₃ objective value (120 µg m⁻³, max. 8 h) when zeroing-out the on-road traffic emissions (SNAP7) for summertime (days with exceedances reduce from 23 to 16 in summer; no exceedances are simulated for winter in the base case); however, this management strategy is hard to take into practice because of the socio-economical implications of road traffic reduction. Moreover, other mobile sources (SNAP8) contribute to 5 days with exceedances of the object value for O₃ (23 days in BC vs. 18 in noSNAP8).

Additionally, other mobile sources (SNAP8) is the sector causing most of the exceedances of the limit values related to NO₂ (200 µg m⁻³, 1 h) and SO₂ (125 µg m⁻³, daily mean) over the IP (playing also a role on PM₁₀ exceedances). In this sense, SNAP8 causes the two exceedances of the limit value of modeled NO₂ and is responsible for six out of the eight exceedances of the daily limit value for SO₂ (125 µg m⁻³) over the domain for summertime (no values over the limit value for NO₂ or SO₂ are modeled during wintertime). SO₂ concentrations over the limit value are found over the Algeciras Bay, and are caused mainly from the contribution of the high sulphur emissions coming from ship fuels. It is noteworthy that the contribution of shipping emissions to the exceedances of the limit value for PM₁₀ is not as large as for SO₂ (in agreement with [92]), since there are components of particulate matter from shipping not directly affected by the sulphur content in the fuels. In this sense, just 2 of the 18 summertime exceedances of the daily mean 50-µg m⁻³ limit value for PM₁₀ are caused by SNAP8 (no exceedances of the PM₁₀ limit value are caused by other mobile sources in wintertime). For particles, combustion in energy generation (SNAP1) is responsible of 5 out of the 18 (27) exceedances of the PM₁₀

limit value for summertime (wintertime), while agriculture (SNAP10) contributes to 2 (6) exceedances of the daily mean $50\text{-}\mu\text{g m}^{-3}$ limit value for summertime (wintertime).

Table 6. Variation in the number of exceedances over the entire IP when zeroing-out the different SNAP sectors (base case minus zeroed-out SNAP sector simulation).

Summer	Summer 2011	w/o SNAP		
Pollutant	Concentration Limit value	Zero-out sector	N exc. BC	N. exc. noSNAP
O ₃	Objective value for O ₃ , 120 $\mu\text{g m}^{-3}$, 8 h	SNAP7	23	16
		SNAP8		18
NO ₂	Limit value for NO ₂ , 200 $\mu\text{g m}^{-3}$, 1 h	SNAP8	2	0
SO ₂	Limit value for SO ₂ , 125 $\mu\text{g m}^{-3}$, 1 day	SNAP1	8	5
		SNAP8		2
PM ₁₀	Limit value for PM ₁₀ , 50 $\mu\text{g m}^{-3}$, 1 day	SNAP1	18	13
		SNAP8		16
		SNAP10		16
Winter	December 2011	w/o SNAP		
Pollutant	Concentration Limit value	Zero-out sector	N exc. BC	N. exc. noSNAP
O ₃	Objective value for O ₃ , 120 $\mu\text{g m}^{-3}$, 8 h	SNAP7	0	0
NO ₂	Limit value for NO ₂ , 200 $\mu\text{g m}^{-3}$, 1 h	SNAP8	0	0
SO ₂	Limit value for SO ₂ , 125 $\mu\text{g m}^{-3}$, 1 day	SNAP1	0	0
		SNAP8		0
PM ₁₀	Limit value for PM ₁₀ , 50 $\mu\text{g m}^{-3}$, 1 day	SNAP4	27	22
		SNAP7		26
		SNAP10		21

4. Discussion and Conclusions

Efficient air quality management requires an accurate identification of pollution sources and of their individual contributions to the ambient pollutant concentrations. To this end, the zero-out methodology has been proposed and applied for the apportionment of atmospheric pollutants in the IP. This method is based on the application of WRF + CHIMERE chemistry transport model coupled to EMEP emissions.

Regarding tropospheric O₃, on-road traffic is the only anthropogenic sector with a noticeable contribution to maximum O₃ levels during summertime (6%) and is responsible for 7 summer days with exceedances in the objective value of 120 $\mu\text{g m}^{-3}$ (max. 8-hr mean) established by the 2008/50/EC directive. These results are in agreement with those of the scientific literature [37,62]. These authors found out that the on-road transport sector (SNAP7) was the largest overall anthropogenic source sector contributing to July 2011 O₃ concentrations in Europe, with non-road transport (SNAP8) contributions ranking second, as in our case (2% contribution to summertime maximum O₃ levels and five exceedances of the objective value). An analogous analysis can be completed for SNAP8 (other mobile sources) with respect to NO₂, with this sector prevailing in the contribution to mean ground-level concentrations during summertime and contributing to the two exceedances of the limit value for the protection of human health for NO₂ (200 $\mu\text{g m}^{-3}$, 1 h) modeled over the IP. The importance of this sector in the IP is larger closer to the major shipping routes and main harbors, with relative contributions varying from 10 to 50% depending on the pollutant (the lowest contribution for particulate matter, the largest for SO₂ and NO₂).

Last, the other anthropogenic sector with a noticeable impact is agriculture. Removing agriculture emissions (SNAP10) contributes to a decrease in PM levels and a simultaneous

increase of SO₂ concentrations. The reduction of the most important source contributing to ammonia emissions controls the formation of ammonium sulphate. Therefore, reducing the levels of ammonia permits the SO₂ to remain in the gas phase. Agriculture contributes to the limit value for the protection of human health regarding PM₁₀ (50 µg m⁻³, daily mean) with 2 exceedances out of 18, while this number increases to 6 out of 27 wintertime exceedances.

With respect to the temporal pattern, in general, the source contribution does not exhibit a strong seasonality, except for particulate matter under the “Other” sector, which includes the external contribution to particle levels. Despite this seasonal behaviour for particulate matter, both gas-phase pollutants and particles exhibit a strong spatial uniformity, since background concentrations in the modeling system are provided by coarse resolution chemistry/climate models that do not allow for a sharp gradient in the background concentrations.

The external contribution of particles to the “Other” sector is mainly composed of mineral matter from Saharan dust. The fact that the boundary contributions to PM₁₀ are larger than for PM_{2.5} for summertime, but lower for wintertime, points to an important role of dust outbreaks over the IP during the summer months, which contributes mainly with large particles. These results are in line with those of Karachamdani et al. [37] for 16 European cities, who indicate that the boundary condition contributions for the Mediterranean cities are larger than for other European cities, ranging from about 40–50% during summertime to 10–15% in wintertime, because those Mediterranean cities were largely influenced by the long-range transport of dust emissions from northern Africa in the summer months.

Locally, the IP undergoes diverse problems related to air quality both during summer and winter. Focusing on the most polluted areas of the target domain (the cities of Madrid, Barcelona, and Algeciras Bay), the impact of road transport (SNAP7) emissions is high for NO₂ ground levels over largely populated areas (Madrid or Barcelona areas), but the concentration of this pollutant is dominated by other mobile sources (such as maritime or airport emissions included in SNAP8). Over coastal areas of the target domain, a poor air quality caused by large NO₂ concentrations can be attributed to shipping routes. In this sense, Merico et al. [87] also highlight the influence of harbor and shipping emissions on air quality of the nearby coastal areas of the Mediterranean.

For SO₂, energy generation (SNAP1) controls the mean levels of this pollutant over most of the areas considered. Valverde et al. [70] indicate that the contribution of power plants to the surface concentration of SO₂ occurs mainly close to the source (<20 km) related to a fumigation process when the emission injection takes place within the planetary boundary layer, but those plumes can reach long distances (>250 km) from the sources.

In the Algeciras Bay, maritime emissions largely contribute to the levels of SO₂. The implementation of low-sulphur fuels in shipping may contribute to substantially reducing the number of exceedances of the limit values for the protection of human health and to reduce several pathologies such as cardiovascular and cancer deaths, childhood asthma, or premature mortality and morbidity [93]. Summertime PM₁₀ and PM_{2.5} levels are dominated by the external contribution of Saharan dust, while for wintertime, agriculture can have a dominant position in Madrid and Barcelona. The important contribution of agriculture to PM levels was highlighted by Lelieveld et al. [94], who stated that this sector is the largest contributor to PM_{2.5} levels in Europe.

Hence, this evaluated contribution has allowed us to identify which sectors contribute most to air pollution problems in the IP. However, it should be borne in mind that the uncertainties associated with several factors (principally, the boundary conditions in the CTMs and emission inventories) can condition the accuracy of the obtained results [37,95]. For instance, Jiménez et al. [17] analyze the impact of initial and boundary conditions over the Levantine coast of the IP, indicating that, despite the influence of initial condition reduces with the spin-up time (a 48-h spin-up time is sufficient to reduce the impact factor of initial conditions to 10% or less), the importance of having accurate boundary conditions becomes essential, since its influence on the results increases with the time of the simulation,

reaching up to $5 \mu\text{g m}^{-3}$ for certain pollutants. With respect to the emission inventories, Baldasano et al. [96] point to industrial facilities as the main sources of uncertainties in emission inventories over the target area.

Nonetheless, this work can provide a very useful contribution to a better understanding of the sensitivity of air pollutants in a complex area such as the IP, and can provide valuable information for the design of mitigation strategies or plans that lead to an improvement in European air quality and the attainment of the SDG over the target area.

Funding: The authors acknowledge the ECCE project (PID2020-115693RB-I00) of the Ministerio de Ciencia e Innovación/Agencia Estatal de Investigación (MCIN/AEI/10.13039/501100011033/) and the European Regional Development Fund (ERDF/FEDER Una manera de hacer Europa). Additionally, the authors thank the reviewers for their valuable contributions and fruitful discussions.

Institutional Review Board Statement: Not applicable.

Informed Consent Statement: Not applicable.

Data Availability Statement: Data are available upon reasonable request from the corresponding author (pedro.jimenezguerrero@um.es)

Conflicts of Interest: The author declares no conflict of interest.

Abbreviations

The following abbreviations are used in this manuscript:

AQI	Air Quality Index
BC	Base Case
BFM	Brute Force Method
CTM	Chemistry Transport Model
EMEP	European Monitoring and Evaluation Programme
IP	Iberian Peninsula
MFB	Mean Fractional Bias
MFE	Mean Fractional Error
MNBE	Mean Normalized Bias Error
MNGE	Mean Normalized Gross Error
NMVOG	Non-Methane Volatile Organic Compounds
SNAP	Selected Nomenclature for Air Pollution
VOC	Volatile Organic Compounds
WRF	Weather Research and Forecasting

References

1. United Nations. *Transforming Our World: The 2030 Agenda for Sustainable Development (A/RES/70/1)*; UN General Assembly: New York, NY, USA, 2015.
2. Tsai, W.T.; Lin, Y.Q. Trend Analysis of Air Quality Index (AQI) and Greenhouse Gas (GHG) Emissions in Taiwan and Their Regulatory Countermeasures. *Environments* **2021**, *8*, 29. [[CrossRef](#)]
3. Kahraman, A.C.; Sivri, N. Comparison of metropolitan cities for mortality rates attributed to ambient air pollution using the AirQ model. *Environ. Sci. Pollut. Res.* **2022**, *29*, 1. doi: 10.1007/s11356-021-18341-1. [[CrossRef](#)] [[PubMed](#)]
4. Osman, T.; Kenawy, E.; Abdrabo, K.I.; Shaw, D.; Alshamndy, A.; Elsharif, M.; Salem, M.; Alwetaishi, M.; Aly, R.M.; Elboshy, B. Voluntary Local Review Framework to Monitor and Evaluate the Progress towards Achieving Sustainable Development Goals at a City Level: Buraidah City, KSA and SDG11 as A Case Study. *Sustainability* **2021**, *13*, 9555. doi: 10.3390/su13179555. [[CrossRef](#)]
5. Pateman, R.; Tuhkanen, H.; Cinderby, S. Citizen Science and the Sustainable Development Goals in Low and Middle Income Country Cities. *Sustainability* **2021**, *13*, 9534. doi: 10.3390/su13179534. [[CrossRef](#)]
6. Cuvelier, C.; Thunis, P.; Vautard, R.; Amann, M.; Bessagnet, B.; Bedogni, M.; Berkowicz, R.; Brandt, J.; Brocheton, F.; Builtjes, P.; et al. CityDelta: A model intercomparison study to explore the impact of emission reductions in European cities in 2010. *Atmos. Environ.* **2007**, *41*, 189–207. [[CrossRef](#)]
7. Ballester, F.; Medina, S.; Boldo, E.; Goodman, P.; Neuberger, M.; Iñiguez, C.; Künzli, N. Reducing ambient levels of fine particulates could substantially improve health: A mortality impact assessment for 26 European cities. *J. Epidemiol. Community Health* **2008**, *62*, 98–105. doi: 10.1136/jech.2007.059857. [[CrossRef](#)]
8. Pope, C.A.; Ezzati, M.; Dockery, D.W. Fine-Particulate Air Pollution and Life Expectancy in the United States. *N. Engl. J. Med.* **2009**, *360*, 376–386. [[CrossRef](#)]

9. Beelen, R.; Raaschou-Nielsen, O.; Stafoggia, M.; Andersen, Z.J.; Weinmayr, G.; Hoffmann, B.; Wolf, K.; Samoli, E.; Fischer, P.; Nieuwenhuijsen, M.; et al. Effects of long-term exposure to air pollution on natural-cause mortality: An analysis of 22 European cohorts within the multicentre ESCAPE project. *Lancet* **2014**, *383*, 785–795. doi: 10.1016/S0140-6736(13)62158-3. [[CrossRef](#)]
10. Héroux, M.E.; Anderson, H.R.; Atkinson, R.; Brunekreef, B.; Cohen, A.; Forastiere, F.; Hurley, F.; Katsouyanni, K.; Krewski, D.; Krzyzanowski, M.; et al. Quantifying the health impacts of ambient air pollutants: recommendations of a WHO/Europe project. *Int. J. Public Health* **2015**, *60*, 619–627. doi: 10.1007/s00038-015-0690-y. [[CrossRef](#)]
11. Tarín-Carrasco, P.; Im, U.; Geels, C.; Palacios-Peña, L.; Jiménez-Guerrero, P. Contribution of fine particulate matter to present and future premature mortality over Europe: A non-linear response. *Environ. Int.* **2021**, *153*, 106517. [[CrossRef](#)]
12. Guzmán, P.; Tarín-Carrasco, P.; Morales-Suárez-Varela, M.; Jiménez-Guerrero, P. Effects of air pollution on dementia over Europe for present and future climate change scenarios. *Environ. Res.* **2022**, *204*, 112012. doi: 10.1016/j.envres.2021.112012. [[CrossRef](#)]
13. Im, U.; Brandt, J.; Geels, C.; Hansen, K.M.; Christensen, J.H.; Andersen, M.S.; Solazzo, E.; Kioutsioukis, I.; Alyuz, U.; Balzarini, A.; et al. Assessment and economic valuation of air pollution impacts on human health over Europe and the United States as calculated by a multi-model ensemble in the framework of AQMEI3. *Atmos. Chem. Phys.* **2018**, *18*, 5967–5989. doi: 10.5194/acp-18-5967-2018. [[CrossRef](#)] [[PubMed](#)]
14. Tarín-Carrasco, P.; Morales-Suárez-Varela, M.; Im, U.; Brandt, J.; Palacios-Peña, L.; Jiménez-Guerrero, P. Isolating the climate change impacts on air-pollution-related-pathologies over central and southern Europe—A modelling approach on cases and costs. *Atmos. Chem. Phys.* **2019**, *19*, 9385–9398. doi: 10.5194/acp-19-9385-2019. [[CrossRef](#)]
15. Monteiro, A.; Carvalho, A.; Ribeiro, I.; Scotto, M.; Barbosa, S.; Alonso, A.; Baldasano, J.; Pay, M.; Miranda, A.; Borrego, C. Trends in ozone concentrations in the Iberian Peninsula by quantile regression and clustering. *Atmos. Environ.* **2012**, *56*, 184–193. [[CrossRef](#)]
16. Baldasano, J.; Pay, M.; Jorba, O.; Gassó, S.; Jiménez-Guerrero, P. An annual assessment of air quality with the CALIOPE modeling system over Spain. *Sci. Total Environ.* **2011**, *409*, 2163–2178. doi: 10.1016/j.scitotenv.2011.01.041. [[CrossRef](#)]
17. Jiménez, P.; Parra, R.; Baldasano, J.M. Influence of initial and boundary conditions for ozone modeling in very complex terrains: A case study in the northeastern Iberian Peninsula. *Environ. Model. Softw.* **2007**, *22*, 1294–1306. [[CrossRef](#)]
18. Vivanco, M.G.; Palomino, L.; Vautard, R.; Bessagnet, B.; Martín, F.; Menut, L.; Jiménez, S. Multi-year assessment of photochemical air quality simulation over Spain. *Environ. Model. Softw.* **2009**, *24*, 63–73. doi: 10.1016/j.envsoft.2008.05.004. [[CrossRef](#)]
19. Borge, R.; López, J.; Lumbreras, J.; Narros, A.; Rodríguez, E. Influence of boundary conditions on CMAQ simulations over the Iberian Peninsula. *Atmos. Environ.* **2010**, *44*, 2681–2695. doi: 10.1016/j.atmosenv.2010.04.044. [[CrossRef](#)]
20. Pay, M.T.; Jiménez-Guerrero, P.; Baldasano, J.M. Assessing sensitivity regimes of secondary inorganic aerosol formation in Europe with the CALIOPE-EU modeling system. *Atmos. Environ.* **2012**, *51*, 146–164. doi: 10.1016/j.atmosenv.2012.01.027. [[CrossRef](#)]
21. Vedrenne, M.; Borge, R.; Lumbreras, J.; Conlan, B.; Rodríguez, M.E.; de Andrés, J.M.; de la Paz, D.; Pérez, J.; Narros, A. An integrated assessment of two decades of air pollution policy making in Spain: Impacts, costs and improvements. *Sci. Total Environ.* **2015**, *527–528*, 351–361. doi: 10.1016/j.scitotenv.2015.05.014. [[CrossRef](#)]
22. Palacios-Peña, L.; Baró, R.; Guerrero-Rascado, J.J.L.; Alados-Arboledas, L.; Brunner, D.; Jiménez-Guerrero, P. Evaluating the representation of aerosol optical properties using an online coupled model over the Iberian Peninsula. *Atmos. Chem. Phys.* **2017**, *17*, 277–296. doi: 10.5194/acp-17-277-2017 [[CrossRef](#)]
23. Guevara, M.; Martínez, F.; Arévalo, G.; Gassó, S.; Baldasano, J.M. An improved system for modelling Spanish emissions: HERMESv2.0. *Atmos. Environ.* **2013**, *81*, 209–221. doi: 10.1016/j.atmosenv.2013.08.053. [[CrossRef](#)]
24. Nunes, R.A.O.; Alvim-Ferraz, M.C.M.; Martins, F.G.; Calderay-Cayetano, F.; Durán-Grados, V.; Moreno-Gutiérrez, J.; Jalkanen, J.P.; Hannuniemi, H.; Sousa, S.I.V. Shipping emissions in the Iberian Peninsula and the impacts on air quality. *Atmos. Chem. Phys.* **2020**, *20*, 9473–9489. [[CrossRef](#)]
25. Querol, X.; Pey, J.; Pandolfi, M.; Alastuey, A.; Cusack, M.; Pérez, N.; Moreno, T.; Viana, M.; Mihalopoulos, N.; Kallos, G.; et al. African dust contributions to mean ambient PM10 mass-levels across the Mediterranean Basin. *Atmos. Environ.* **2009**, *43*, 4266–4277. [[CrossRef](#)]
26. Carvalho, A.; Monteiro, A.; Solman, S.; Miranda, A.; Borrego, C. Climate-driven changes in air quality over Europe by the end of the 21st century, with special reference to Portugal. *Environ. Sci. Policy* **2010**, *13*, 445–458. [[CrossRef](#)]
27. Jiménez-Guerrero, P.; Montávez, J.P.; Gómez-Navarro, J.J.; Jerez, S.; Lorente-Plazas, R. Impacts of climate change on ground level gas-phase pollutants and aerosols in the Iberian Peninsula for the late XXI century. *Atmos. Environ.* **2012**, *55*, 483–495. [[CrossRef](#)]
28. Jiménez-Guerrero, P.; Gómez-Navarro, J.J.J.; Baró, R.; Lorente, R.; Ratola, N.; Montávez, J.P. Is there a common pattern of future gas-phase air pollution in Europe under diverse climate change scenarios? *Clim. Chang.* **2013**, *121*, 661–671. [[CrossRef](#)]
29. Jiménez-Guerrero, P.; Jerez, S.; Montávez, J.P.; Trigo, R.M. Uncertainties in future ozone and PM10 projections over Europe from a regional climate multiphysics ensemble. *Geophys. Res. Lett.* **2013**, *40*, 5764–5769. [[CrossRef](#)]
30. Monteiro, A.; Sá, E.; Fernandes, A.; Gama, C.; Sorte, S.; Borrego, C.; Lopes, M.; Russo, M.A. How healthy will be the air quality in 2050? *Air Qual. Atmos. Health* **2018**, *11*, 353–362. [[CrossRef](#)]
31. Vautard, R.; Colette, A.; van Meijgaard, E.; Meleux, F.; van Oldenborgh, G.J.; Otto, F.; Tobin, I.; Yiou, P. Attribution of Wintertime Anticyclonic Stagnation Contributing to Air Pollution in Western Europe. *Bull. Am. Meteorol. Soc.* **2018**, *99*, S70–S75. [[CrossRef](#)]
32. Yarwood, G.; Emery, C.; Jung, J.; Nopmongkol, U.; Sakulyanontvittaya, T. A method to represent ozone response to large changes in precursor emissions using high-order sensitivity analysis in photochemical models. *Geosci. Model Dev.* **2013**, *6*, 1601–1608. [[CrossRef](#)]

33. Pisoni, E.; Albrecht, D.; Mara, T.; Rosati, R.; Tarantola, S.; Thunis, P. Application of uncertainty and sensitivity analysis to the air quality SHERPA modelling tool. *Atmos. Environ.* **2018**, *183*, 84–93. [[CrossRef](#)]
34. Koo, B.; Wilson, G.M.; Morris, R.E.; Dunker, A.M.; Yarwood, G. Comparison of Source Apportionment and Sensitivity Analysis in a Particulate Matter Air Quality Model. *Environ. Sci. Technol.* **2009**, *43*, 6669–6675. [[CrossRef](#)] [[PubMed](#)]
35. Kranenburg, R.; Segers, A.J.; Hendriks, C.; Schaap, M. Source apportionment using LOTOS-EUROS: Module description and evaluation. *Geosci. Model Dev.* **2013**, *6*, 721–733. [[CrossRef](#)]
36. Clappier, A.; Belis, C.A.; Pernigotti, D.; Thunis, P. Source apportionment and sensitivity analysis: Two methodologies with two different purposes. *Geosci. Model Dev.* **2017**, *10*, 4245–4256. [[CrossRef](#)]
37. Karamchandani, P.; Long, Y.; Pirovano, G.; Balzarini, A.; Yarwood, G. Source-sector contributions to European ozone and fine PM in 2010 using AQMEII modeling data. *Atmos. Chem. Phys.* **2017**, *17*, 5643–5664. [[CrossRef](#)]
38. Wang, L.; Wei, Z.; Wei, W.; Fu, J.S.; Meng, C.; Ma, S. Source apportionment of PM_{2.5} in top polluted cities in Hebei, China using the CMAQ model. *Atmos. Environ.* **2015**, *122*, 723–736. [[CrossRef](#)]
39. Huang, Y.; Deng, T.; Li, Z.; Wang, N.; Yin, C.; Wang, S.; Fan, S. Numerical simulations for the sources apportionment and control strategies of PM_{2.5} over Pearl River Delta, China, part I: Inventory and PM_{2.5} sources apportionment. *Sci. Total Environ.* **2018**, *634*, 1631–1644. [[CrossRef](#)]
40. Baker, K.; Woody, M.; Tonnesen, G.; Hutzell, W.; Pye, H.; Beaver, M.; Pouliot, G.; Pierce, T. Contribution of regional-scale fire events to ozone and PM_{2.5} air quality estimated by photochemical modeling approaches. *Atmos. Environ.* **2016**, *140*, 539–554. [[CrossRef](#)]
41. Han, X.; Zhang, M.; Zhu, L.; Skorokhod, A. Assessment of the impact of emissions reductions on air quality over North China Plain. *Atmos. Pollut. Res.* **2016**, *7*, 249–259. [[CrossRef](#)]
42. Klemp, J.B.; Skamarock, W.C.; Dudhia, J. Conservative Split-Explicit Time Integration Methods for the Compressible Nonhydrostatic Equations. *Mon. Weather. Rev.* **2007**, *135*, 2897–2913. [[CrossRef](#)]
43. Skamarock, W.C.; Klemp, J.B.; Dudhia, J.; Gill, D.O.; Barker, D.M.; Wang, W.; Powers, J.G. *A Description of the Advanced Research WRF Version 3*; note-475+ STR; NCAR Technical Report: Boulder, CO, USA, 2008.
44. Dee, D.P.; Uppala, S.M.; Simmons, A.J.; Berrisford, P.; Poli, P.; Kobayashi, S.; Andrae, U.; Balmaseda, M.A.; Balsamo, G.; Bauer, P.; et al. The ERA-Interim reanalysis: Configuration and performance of the data assimilation system. *Q. J. R. Meteorol. Soc.* **2011**, *137*, 553–597. [[CrossRef](#)]
45. Menut, L.; Bessagnet, B.; Khvorostyanov, D.; Beekmann, M.; Blond, N.; Colette, A.; Coll, I.; Curci, G.; Foret, G.; Hodzic, A.; et al. CHIMERE 2013: A model for regional atmospheric composition modelling. *Geosci. Model Dev.* **2013**, *6*, 981–1028. [[CrossRef](#)]
46. Derognat, C.; Beekmann, M.; Baeumle, M.; Martin, D.; Schmidt, H. Effect of biogenic volatile organic compound emissions on tropospheric chemistry during the Atmospheric Pollution Over the Paris Area (ESQUIF) campaign in the Ile-de-France region. *J. Geophys. Res.* **2003**, *108*, 8560. [[CrossRef](#)]
47. Hong, S.; Lim, J.O.J. The WRF Single-Moment 6-Class Microphysics Scheme (WSM6). *Asia-Pac. J. Atmos. Sci.* **2006**, *42*, 129–151.
48. Hong, S.Y.; Noh, Y.; Dudhia, J. A New Vertical Diffusion Package with an Explicit Treatment of Entrainment Processes. *Mon. Weather. Rev.* **2006**, *134*, 2318–2341. [[CrossRef](#)]
49. Nenes, A.; Pandis, S.N.; Pilinis, C. ISORROPIA: A New Thermodynamic Equilibrium Model for Multiphase Multicomponent Inorganic Aerosols. *Aquat. Geochem.* **1998**, *4*, 123–152. [[CrossRef](#)]
50. Collins, W.D.; Rasch, P.J.; Boville, B.A.; Hack, J.J.; McCaa, J.R.; Williamson, D.L.; Kiehl, J.T.; Briegleb, B.; Bitz, C.; Lin, S.J.; et al. *Description of the NCAR Community Atmosphere Model (CAM 3.0)*; Note NCAR/TN-464+ STR; NCAR Technical Report; NCAR: Boulder, CO, USA, 2004; Volume 226, 1326–1334.
51. Bessagnet, B.; Menut, L.; Curci, G.; Hodzic, A.; Guillaume, B.; Lioussse, C.; Moukhtar, S.; Pun, B.; Seigneur, C.; Schulz, M. Regional modeling of carbonaceous aerosols over Europe—Focus on secondary organic aerosols. *J. Atmos. Chem.* **2008**, *61*, 175–202. [[CrossRef](#)]
52. Chen, F.; Dudhia, J. Coupling an Advanced Land Surface-Hydrology Model with the Penn State-NCAR MM5 Modeling System. Part I: Model Implementation and Sensitivity. *Mon. Weather. Rev.* **2001**, *129*, 569–585. [[CrossRef](#)]
53. Kain, J.S. The Kain-Fritsch convective parameterization: An update. *J. Appl. Meteorol.* **2004**, *43*, 170–181. doi: 10.1175/1520-0450(2004)043<0170:TKCPAU>2.0.CO;2. [[CrossRef](#)]
54. Vestreng, V.; Ntziachristos, L.; Semb, A.; Reis, S.; Isaksen, I.S.; Tarrasón, L. Evolution of NO_x emissions in Europe with focus on road transport control measures. *Atmos. Chem. Phys.* **2009**, *9*, 1503–1520. [[CrossRef](#)]
55. Guenther, A.; Karl, T.; Harley, P.; Wiedinmyer, C.; Palmer, P.I.; Geron, C. Estimates of global terrestrial isoprene emissions using MEGAN (Model of Emissions of Gases and Aerosols from Nature). *Atmos. Chem. Phys.* **2006**, *6*, 3181–3210. [[CrossRef](#)]
56. Folberth, G.A.; Hauglustaine, D.A.; Lathière, J.; Brocheton, F. Interactive chemistry in the Laboratoire de Météorologie Dynamique general circulation model: Model description and impact analysis of biogenic hydrocarbons on tropospheric chemistry. *Atmos. Chem. Phys.* **2006**, *6*, 2273–2319. [[CrossRef](#)]
57. Szopa, S.; Foret, G.; Menut, L.; Cozic, A. Impact of large scale circulation on European summer surface ozone and consequences for modelling forecast. *Atmos. Environ.* **2009**, *43*, 1189–1195. [[CrossRef](#)]
58. Jiménez-Guerrero, P.; Ratola, N. Influence of the North Atlantic oscillation on the atmospheric levels of benzo[a]pyrene over Europe. *Clim. Dyn.* **2021**, *57*, 1173–1186. [[CrossRef](#)]

59. Borge, R.; Lumberras, J.; Vardoulakis, S.; Kassomenos, P.; Rodríguez, E. Analysis of long-range transport influences on urban PM10 using two-stage atmospheric trajectory clusters. *Atmos. Environ.* **2007**, *41*, 4434–4450. doi: [CrossRef]
60. Salvador, P.; Artíñano, B.; Molero, F.; Viana, M.; Pey, J.; Alastuey, A.; Querol, X. African dust contribution to ambient aerosol levels across central Spain: Characterization of long-range transport episodes of desert dust. *Atmos. Res.* **2013**, *127*, 117–129. [CrossRef]
61. Brandt, J.; Silver, J.D.; Christensen, J.H.; Andersen, M.S.; Bønløkke, J.H.; Sigsgaard, T.; Geels, C.; Gross, A.; Hansen, A.B.; Hansen, K.M.; et al. Contribution from the ten major emission sectors in Europe and Denmark to the health-cost externalities of air pollution using the EVA model system – an integrated modelling approach. *Atmos. Chem. Phys.* **2013**, *13*, 7725–7746. [CrossRef]
62. Tagaris, E.; Sotiropoulou, R.E.P.; Gounaris, N.; Andronopoulos, S.; Vlachogiannis, D. Effect of the Standard Nomenclature for Air Pollution (SNAP) Categories on Air Quality over Europe. *Atmosphere* **2015**, *6*, 1119–1128. [CrossRef]
63. Arunachalam, S.; Valencia, A.; Akita, Y.; Serre, M.L.; Omary, M.; Garcia, V.; Isakov, V. A Method for Estimating Urban Background Concentrations in Support of Hybrid Air Pollution Modeling for Environmental Health Studies. *Int. J. Environ. Res. Public Health* **2014**, *11*, 10518–10536. [CrossRef]
64. Tørseth, K.; Aas, W.; Breivik, K.; Fjæraa, A.M.; Fiebig, M.; Hjellbrekke, A.G.; Lund Myhre, C.; Solberg, S.; Yttri, K.E. Introduction to the European Monitoring and Evaluation Programme (EMEP) and observed atmospheric composition change during 1972–2009. *Atmos. Chem. Phys.* **2012**, *12*, 5447–5481. [CrossRef]
65. Boylan, J.W.; Russell, A.G. PM and light extinction model performance metrics, goals, and criteria for three-dimensional air quality models. *Atmos. Environ.* **2006**, *40*, 4946–4959. Special issue on Model Evaluation: Evaluation of Urban and Regional Eulerian Air Quality Models, [CrossRef]
66. Zhang, H.; Chen, G.; Hu, J.; Chen, S.H.; Wiedinmyer, C.; Kleeman, M.; Ying, Q. Evaluation of a seven-year air quality simulation using the Weather Research and Forecasting (WRF)/Community Multiscale Air Quality (CMAQ) models in the eastern United States. *Sci. Total Environ.* **2014**, *473–474*, 275–285. [CrossRef] [PubMed]
67. Gao, M.; Guttikunda, S.K.; Carmichael, G.R.; Wang, Y.; Liu, Z.; Stanier, C.O.; Saide, P.E.; Yu, M. Health impacts and economic losses assessment of the 2013 severe haze event in Beijing area. *Sci. Total Environ.* **2015**, *511*, 553–561. [CrossRef]
68. Sammartino, S.; García Lafuente, J.; Sánchez Garrido, J.; De los Santos, F.; Álvarez Fanjul, E.; Naranjo, C.; Bruno, M.; Calero, C. A numerical model analysis of the tidal flows in the Bay of Algeciras, Strait of Gibraltar. *Cont. Shelf Res.* **2014**, *72*, 34–46. [CrossRef]
69. Dios, M.; Souto, J.; Casares, J. Experimental development of CO₂, SO₂ and NO_x emission factors for mixed lignite and subbituminous coal-fired power plant. *Energy* **2013**, *53*, 40–51. [CrossRef]
70. Valverde, V.; Pay, M.T.; Baldasano, J.M. A model-based analysis of SO₂ and NO₂ dynamics from coal-fired power plants under representative synoptic circulation types over the Iberian Peninsula. *Sci. Total Environ.* **2016**, *541*, 701–713. [CrossRef]
71. Kushta, J.; Georgiou, G.K.; Proestos, Y.; Christoudias, T.; Thunis, P.; Savvides, C.; Papadopoulos, C.; Lelieveld, J. Evaluation of EU air quality standards through modeling and the FAIRMODE benchmarking methodology. *Air Qual. Atmos. Health* **2019**, *12*, 73–86. [CrossRef]
72. Terrenoire, E.; Bessagnet, B.; Rouïl, L.; Tognet, F.; Pirovano, G.; Létinois, L.; Beauchamp, M.; Colette, A.; Thunis, P.; Amann, M.; et al. High-resolution air quality simulation over Europe with the chemistry transport model CHIMERE. *Geosci. Model Dev.* **2015**, *8*, 21–42. [CrossRef]
73. Mateos, D.; Cachorro, V.; Toledano, C.; Burgos, M.; Bennouna, Y.; Torres, B.; Fuertes, D.; González, R.; Guirado, C.; Calle, A.; et al. Columnar and surface aerosol load over the Iberian Peninsula establishing annual cycles, trends, and relationships in five geographical sectors. *Sci. Total Environ.* **2015**, *518–519*, 378–392. [CrossRef]
74. Jiménez-Guerrero, P.; Pérez, C.; Jorba, O.; Baldasano, J.M. Contribution of Saharan dust in an integrated air quality system and its on-line assessment. *Geophys. Res. Lett.* **2008**, *35*, L03814. [CrossRef]
75. Stein, A.F.; Wang, Y.; de la Rosa, J.D.; de la Campa, A.M.S.; Castell, N.; Draxler, R.R. Modeling PM10 Originating from Dust Intrusions in the Southern Iberian Peninsula Using HYSPLIT. *Weather. Forecast.* **2011**, *26*, 236–242. [CrossRef]
76. de la Paz, D.; Vedrenne, M.; Borge, R.; Lumberras, J.; Manuel de Andrés, J.; Pérez, J.; Rodríguez, E.; Karanasiou, A.; Moreno, T.; Boldo, E.; et al. Modelling Saharan dust transport into the Mediterranean basin with CMAQ. *Atmos. Environ.* **2013**, *70*, 337–350. [CrossRef]
77. Jiménez, P.; Baldasano, J.M. Ozone response to precursor controls in very complex terrains: Use of photochemical indicators to assess O₃-NO_x-VOC sensitivity in the northeastern Iberian Peninsula. *J. Geophys. Res. Atmos.* **2004**, *109*, 1–20. [CrossRef]
78. Castell, N.; Stein, A.F.; Mantilla, E.; Salvador, R.; Millán, M. Evaluation of the use of photochemical indicators to assess ozone—NO_x—VOC sensitivity in the Southwestern Iberian Peninsula. *J. Atmos. Chem.* **2009**, *63*, 73–91. [CrossRef]
79. Marmer, E.; Dentener, F.; Aardenne, J.v.; Cavalli, F.; Vignati, E.; Velchev, K.; Hjorth, J.; Boersma, F.; Vinken, G.; Mihalopoulos, N.; et al. What can we learn about ship emission inventories from measurements of air pollutants over the Mediterranean Sea? *Atmos. Chem. Phys.* **2009**, *9*, 6815–6831. [CrossRef]
80. Carrillo-Torres, E.R.; Hernández-Paniagua, I.Y.; Mendoza, A. Use of Combined Observational- and Model-Derived Photochemical Indicators to Assess the O₃-NO_x-VOC System Sensitivity in Urban Areas. *Atmosphere* **2017**, *8*, 22. doi: [CrossRef]
81. Renner, E.; Wolke, R. Modelling the formation and atmospheric transport of secondary inorganic aerosols with special attention to regions with high ammonia emissions. *Atmos. Environ.* **2010**, *44*, 1904–1912. [CrossRef]
82. Kyrkilis, G.; Chaloulakou, A.; Kassomenos, P.A. Development of an aggregate Air Quality Index for an urban Mediterranean agglomeration: Relation to potential health effects. *Environ. Int.* **2007**, *33*, 670–676. [CrossRef]

83. Borrego, C.; Monteiro, A.; Martins, H.; Ferreira, J.; Fernandes, A.P.; Rafael, S.; Miranda, A.I.; Guevara, M.; Baldasano, J.M. Air quality plan for ozone: An urgent need for North Portugal. *Air Qual. Atmos. Health* **2016**, *9*, 447–460. [[CrossRef](#)]
84. Derwent, R.G.; Utembe, S.R.; Jenkin, M.E.; Shallcross, D.E. Tropospheric ozone production regions and the intercontinental origins of surface ozone over Europe. *Atmos. Environ.* **2015**, *112*, 216–224. [[CrossRef](#)]
85. Gencarelli, C.N.; De Simone, F.; Hedgecock, I.M.; Sprovieri, F.; Pirrone, N. Development and application of a regional-scale atmospheric mercury model based on WRF/Chem: A Mediterranean area investigation. *Environ. Sci. Pollut. Res.* **2014**, *21*, 4095–4109. [[CrossRef](#)] [[PubMed](#)]
86. Aksoyoglu, S.; Baltensperger, U.; Prévôt, A.S.H. Contribution of ship emissions to the concentration and deposition of air pollutants in Europe. *Atmos. Chem. Phys.* **2016**, *16*, 1895–1906. [[CrossRef](#)]
87. Merico, E.; Donato, A.; Gambaro, A.; Cesari, D.; Gregoris, E.; Barbaro, E.; Dinoi, A.; Giovanelli, G.; Masieri, S.; Contini, D. Influence of in-port ships emissions to gaseous atmospheric pollutants and to particulate matter of different sizes in a Mediterranean harbour in Italy. *Atmos. Environ.* **2016**, *139*, 1–10. [[CrossRef](#)]
88. Valverde, V.; Pay, M.T.; Baldasano, J.M. Ozone attributed to Madrid and Barcelona on-road transport emissions: Characterization of plume dynamics over the Iberian Peninsula. *Sci. Total Environ.* **2016**, *543*, 670–682. doi: [[CrossRef](#)] [[PubMed](#)]
89. Cesari, D.; Amato, F.; Pandolfi, M.; Alastuey, A.; Querol, X.; Contini, D. An inter-comparison of PM10 source apportionment using PCA and PMF receptor models in three European sites. *Environ. Sci. Pollut. Res.* **2016**, *23*, 15133–15148. [[CrossRef](#)]
90. Palomares-Salas, J.C.; González-de-la Rosa, J.J.; Agüera-Pérez, A.; Sierra-Fernández, J.M.; Florencias-Oliveros, O. Forecasting PM10 in the Bay of Algeciras Based on Regression Models. *Sustainability* **2019**, *11*, 968. [[CrossRef](#)]
91. Pérez, N.; Pey, J.; Reche, C.; Cortés, J.; Alastuey, A.; Querol, X. Impact of harbour emissions on ambient PM10 and PM2.5 in Barcelona (Spain): Evidences of secondary aerosol formation within the urban area. *Sci. Total Environ.* **2016**, *571*, 237–250. [[CrossRef](#)]
92. Jonson, J.E.; Jalkanen, J.P.; Johansson, L.; Gauss, M.; Denier van der Gon, H.A.C. Model calculations of the effects of present and future emissions of air pollutants from shipping in the Baltic Sea and the North Sea. *Atmos. Chem. Phys.* **2015**, *15*, 783–798. [[CrossRef](#)]
93. Sofiev, M.; Winebrake, J.J.; Johansson, L.; Carr, E.W.; Prank, M.; Soares, J.; Vira, J.; Kouznetsov, R.; Jalkanen, J.P.; Corbett, J.J. Cleaner fuels for ships provide public health benefits with climate tradeoffs. *Nat. Commun.* **2018**, *9*, 406. [[CrossRef](#)]
94. Lelieveld, J.; Evans, J.S.; Fnais, M.; Giannadaki, D.; Pozzer, A. The contribution of outdoor air pollution sources to premature mortality on a global scale. *Nature* **2015**, *525*, 367–371. [[CrossRef](#)] [[PubMed](#)]
95. Solazzo, E.; Bianconi, R.; Hogrefe, C.; Curci, G.; Tuccella, P.; Alyuz, U.; Balzarini, A.; Baro, R.; Bellasio, R.; Bieser, J.; et al. Evaluation and error apportionment of an ensemble of atmospheric chemistry transport modeling systems: Multivariable temporal and spatial breakdown. *Atmos. Chem. Phys.* **2017**, *17*, 3001–3054. [[CrossRef](#)] [[PubMed](#)]
96. Baldasano, J.M.; Güereca, L.P.; López, E.; Gassó, S.; Jimenez-Guerrero, P. Development of a high-resolution (1 km × 1 km, 1h) emission model for Spain: The High-Selective Resolution Modelling Emission System (HERMES). *Atmos. Environ.* **2008**, *42*, 7215–7233. [[CrossRef](#)]